Journal of Microbiology, Immunology and Infection 58 (2025) 77–85

Contents lists available at ScienceDirect

Journal of Microbiology, Immunology and Infection

journal homepage: www.e-jmii.com

Identification of *Staphylococcus aureus*, *Enterococcus faecium*, *Klebsiella pneumoniae*, *Pseudomonas aeruginosa* and *Acinetobacter baumannii* from Raman spectra by Artificial Intelligent Raman Detection and Identification System (AIRDIS) with machine learning

Yu-Tzu Lin [a,1], Hsiu-Hsien Lin [b,1], Chih-Hao Chen [c], Kun-Hao Tseng [b], Pang-Chien Hsu [b], Ya-Lun Wu [d], Wei-Cheng Chang [e], Nai-Shun Liao [e], Yi-Fan Chou [e], Chun-Yi Hsu [e], Yu-Hui Liao [e], Mao-Wang Ho [c], Shih-Sheng Chang [d], Po-Ren Hsueh [b,c,*], Der-Yang Cho [f]

[a] *Department of Medical Laboratory Science and Biotechnology, China Medical University, Taichung, Taiwan*
[b] *Department of Laboratory Medicine, China Medical University Hospital, China Medical University, Taichung, Taiwan*
[c] *Division of Infectious Diseases, Department of Internal Medicine, China Medical University Hospital, China Medical University, Taichung, Taiwan*
[d] *AI Innovation Center, China Medical University Hospital, Taichung City, Taiwan*
[e] *ITRUST MedTech Inc., Hsinchu, Taiwan*
[f] *Department of Neurosurgery, China Medical University Hospital, Taichung, Taiwan*

ARTICLE INFO

Keywords:
Raman spectroscopy
MALDI-TOF MS
Artificial intelligence
Machine learning
Species identification

ABSTRACT

Background: Rapid and accurate identification of bacteria is required in order to develop effective treatment strategies. Traditional culture-based methods are time-consuming, while MALDI-TOF MS is expensive. The Raman spectroscopy, due to its relatively cost-effectiveness, offers a promising alternative for bacterial identification. However, its clinical utility still requires further validation.

Methods: In this study, the artificial intelligent Raman detection and identification system (AIRDIS) was implemented to identify bacterial species, including *Staphylococcus aureus* (n = 1290), *Enterococcus faecium* (n = 1020), *Klebsiella pneumoniae* (n = 1366), *Pseudomonas aeruginosa* (n = 1067), and *Acinetobacter baumannii* (n = 811). Raman spectra were collected, preprocessed, and analyzed by machine learning (ML).

Results: After training on 24,420 Raman spectra from 1221 isolates and testing on 4333 isolates, the AIRDIS demonstrated an area under the curve (AUC) of 0.99 for Gram classification, with accuracies of 97.64 % for Gram-positive bacteria and 98.86 % for Gram-negative bacteria. Spectral differences between Gram-positive and Gram-negative bacteria were linked to structural variations in their cell walls, such as peptidoglycan and lipopolysaccharides. At the species level, *S. aureus*, *E. faecium*, *K. pneumoniae*, *P. aeruginosa*, and *A. baumannii* were identified with high accuracy, ranging from 94.76 % to 96.88 %, with all species achieving an AUC of 0.99.

Conclusions: Validation with a large number of clinical isolates demonstrated Raman spectroscopy combined with ML excels in identification of five bacterial species associated with multidrug resistance. This finding confirms the clinical utility of the system while laying a solid foundation for the future development of antimicrobial resistance prediction models.

1. Introduction

Bacterial infections have long been a critical issue in global public health and remain one of the leading causes of mortality worldwide. A systematic investigation conducted in 2019 revealed that 13.7 million deaths were associated with infectious diseases.[1] Additional studies also indicate that over 20 % of annual global deaths are linked to infections.[2,3] Therefore, reducing the mortality burden caused by

* Corresponding author. Departments of Laboratory Medicine and Internal Medicine, China Medical University Hospital, School of Medicine, China Medical University, Taichung, Taiwan.
E-mail address: hsporen@gmail.com (P.-R. Hsueh).
[1] These authors contributed equally to this work.

https://doi.org/10.1016/j.jmii.2024.11.014
Received 22 November 2024; Received in revised form 27 November 2024; Accepted 28 November 2024
Available online 29 November 2024

infections is an urgent priority for global public health. Rapid and accurate bacterial identification in clinical infections is essential for precise diagnosis, effective treatment, and robust public health management. Traditionally, culture-based methods have been regarded as the gold standard for bacterial detection and identification.[4] Although automated identification systems, such as VITEK® 2 (bioMe'rieux, Marcy l'Etoile, France) and BD Phoenix™ (Becton-Dickinson Microbiology Systems, Sparks, MD, USA), have improved throughput, they still require an additional 24–48 h for definitive identification.[5] Matrix-assisted laser desorption ionization-time of flight mass spectrometry (MALDI-TOF MS) rapidly ionizes bacterial proteins directly from cultured colonies using laser pulses, generating a species-specific protein fingerprint. This technology is now widely employed in clinical microbiology laboratories. Each sample analysis requires only 5–7 min, typically allowing results to be available within 12–24 h after sample receipt.[5] However, the MALDI-TOF MS system comes with an initial cost exceeding $300,000 USD, along with substantial annual maintenance expenses, making it a significant financial burden for small to medium-sized hospitals. Other identification methods, such as molecular-based approaches, offer shorter processing times but still require additional equipment or manual steps, thereby increasing the workload of clinical microbiologists.[6] Given these challenges, there is an urgent need to develop a rapid, accurate, and cost-effective bacterial identification system.

Raman spectroscopy, due to its label-free, non-invasive nature and high sensitivity, is considered to hold significant potential for bacterial identification.[7–9] When a monochromatic laser beam interacts with a sample, scattering occurs. If the photon energy of the scattered light is equal to that of the incident light, it is termed elastic scattering or Rayleigh scattering. However, if the energy of the scattered light differs from that of the incident light, it is referred to as inelastic scattering or Raman scattering.[10] Raman scattering photons can either loss or gain energy. If the energy of the scattered photon is lower than that of the incident photon, the phenomenon is termed Stokes scattering. In contrast, if the scattered photon has higher energy, it is referred to as anti-Stokes scattering.[11] The frequency difference between the incident and scattered photons is known as the Raman shift.[12] The observation of Raman scattering is often limited by high fluorescence excitation intensity.[13] To overcome this limitation, surface-enhanced Raman scattering (SERS) is employed to amplify Raman signals, thereby enhancing sensitivity. SERS achieves signal amplification through the enhancement of the electromagnetic field at metal surfaces and the charge-transfer interactions between the metal and the molecules.[14]

Due to the complexity of Raman spectra and the subtle differences between the spectra of different bacterial species, machine learning (ML) is often employed for data processing. Currently, several bacterial identification models combining Raman spectroscopy with deep learning techniques, such as convolutional neural networks (CNNs), have been developed.[15] Numerous studies on these applications have been reported; however, they often fail to include clinically significant antibiotic-resistant species and typically involve a limited number of isolates.[9,16,17]

This study aims to develop a system, referred to as the Artificial Intelligent Raman Detection and Identification System (AIRDIS), which integrates Raman spectroscopy and ML to identify clinically significant bacterial species associated with multidrug resistance, including *Staphylococcus aureus*, *Enterococcus faecium*, *Klebsiella pneumoniae*, *Pseudomonas aeruginosa*, and *Acinetobacter baumannii*. The system is designed to facilitate the future development of antimicrobial resistance prediction models.

2. Materials and methods

2.1. Bacterial isolates

To evaluate the clinical performance of the AIRDIS and its microbial identification software (ITRUST MedTech Inc., Hsinchu, Taiwan), this study tested five clinically most encountered bacterial species. These species isolates included *S. aureus* (n = 1290), *E. faecium* (n = 1020), *K. pneumoniae* (n = 1366), *P. aeruginosa* (n = 1067), and *A. baumannii* (n = 811) and were collected from positive blood cultures from clinical laboratory of China Medical University Hospital (CMUH) between 2021 and 2023 (n = 2516) and from the Surveillance of Multicenter Antimicrobial Resistance in Taiwan (SMART) between 2017 and 2020 (n = 3038) (Table 1).[18–21] Bacterial isolates were cultured on trypticase soy agar (TSA) with 5 % sheep blood (Becton-Dickinson Microbiology Systems) at 37 °C for 16–18 h. This process involved both the direct inoculation of specimens onto blood agar plates and subculturing from positive blood culture bottles. The species identification of the isolates was subsequently confirmed using matrix-assisted laser desorption/ionization time-of-flight mass spectrometry (MALDI-TOF MS) Biotyper system (Bruker Microflex LT/SH, Bruker Daltonics GmbH).

2.2. Study workflow

To establish and investigate the feasibility of applying Raman spectrum combined with deep learning for clinical bacterial identification, this study employed the AIRDIS to collect bacterial spectral data. Species identification was concurrently performed following standard clinical workflows using the MALDI-TOF MS Biotyper system. The species identification results were used as labels for the bacterial Raman spectra, facilitating the deep learning analysis and validation as shown in Fig. 1.

2.3. Bacterial isolates

Among 5554 isolates, 1221 were randomly selected for training, including 150 *S. aureus*, 150 *E. faecium*, 150 *K. pneumoniae*, 150 *P. aeruginosa*, and 150 *A. baumannii* isolates from SMART program, as well as 125 *S. aureus*, 106 *E. faecium*, 124 *K. pneumoniae*, 97 *P. aeruginosa*, and 19 *A. baumannii* isolates from CMUH. The remaining 4333 isolates were used for testing.

2.4. Preparation of Raman samples

The isolates were incubated on blood agar plates at 37 °C for 16–18 h. A single colony then selected and mixed with a silver nanoparticle SERS colloid (ITRUST MedTech Inc.) on a stainless-steel substrate (ITRUST MedTech Inc.), resulting in a circular spot approximately 2–3 mm wide following rapid air-drying. After drying, the bacterial isolates were excited with a 785 nm laser,[22] which induced Raman scattering from the bacterial cells. In the application of SERS technology, the colloidal silver nanoparticles interact directly with the bacterial strains. By positioning the bacterial cells near the plasmonic silver nanoparticles, the enhanced electromagnetic field from the nanoparticles amplifies the Raman signal, enabling the acquisition of representative Raman fingerprint spectra of the bacteria, as shown in Fig. 2.

Table 1
Bacteria isolates evaluated in this study.

Organism	No. of isolates collected	
	CMUH	SMART
S. aureus	664	626
E. faecium	383	637
K. pneumoniae	760	606
P. aeruginosa	514	553
A. baumannii	195	616
Subtotal	2516	3038
Total	5554	

CMUH, China Medical University Hospital; SMART, Surveillance of Multicenter Antimicrobial Resistance in Taiwan.

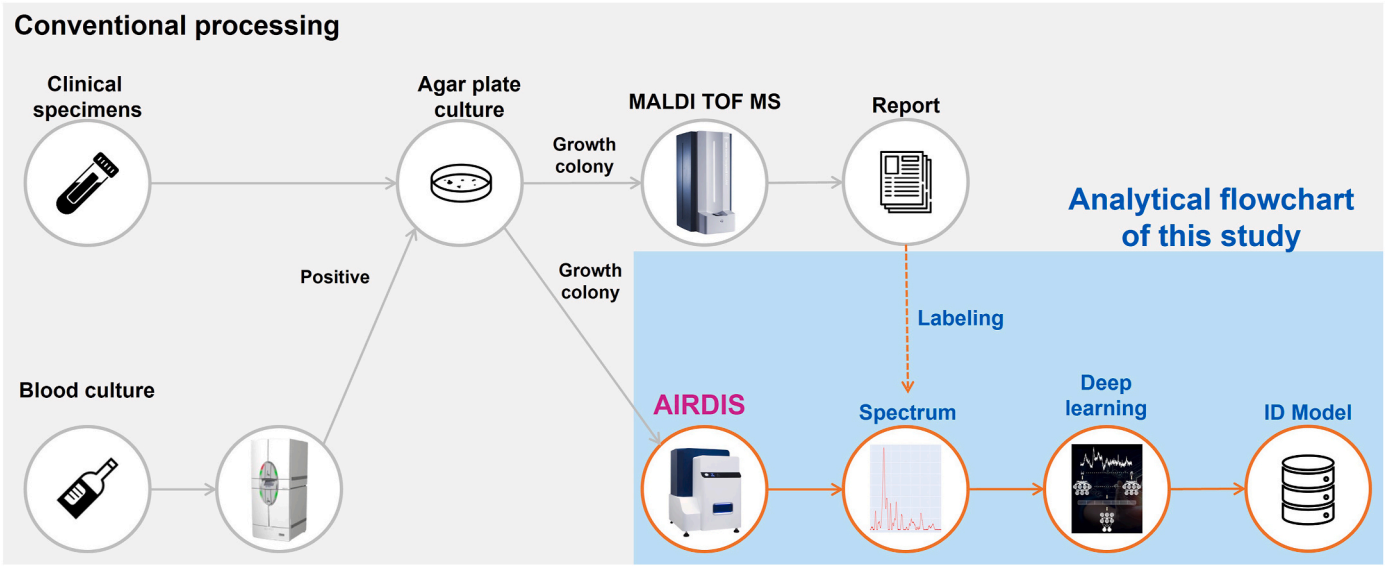

Fig. 1. Workflow of this study. Bacteria cultured from blood specimens or positive blood culture bottles were analyzed using MALDI-TOF MS and AIRDIS, respectively. The identification results from MALDI-TOF MS were used as labels for the bacterial Raman spectra to train and validate the deep learning model.

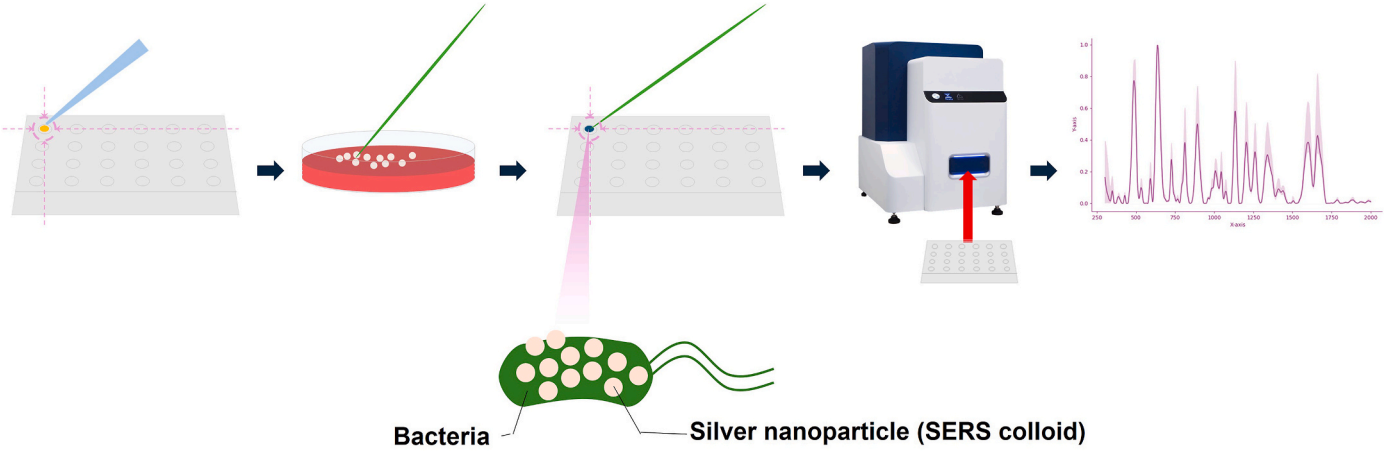

Fig. 2. Schema of the label-free SERS detection of bacteria. The acquisition of bacterial Raman spectra followed these steps: (1) a reagent was dispensed onto a reflective substrate, (2) a single bacterial colony was picked using a sterile loop, (3) the bacteria were mixed with the reagent on the substrate, (4) the mixture was allowed to air-dry, and (5) the sample was analyzed to obtain the Raman spectra.

2.5. Raman measurements

The AIRDIS was employed to record Raman scattering signals, utilizing a 1-s integration time and laser power adjusted between 1 and 500 mW during data collection. The ring-shaped region was selected as the measurement area, and spectra were collected from 20 randomly chosen points within this region to minimize the coffee-ring effect and enhance reproducibility. The coffee-ring effect is a common phenomenon in SERS measurements, where the colloidal particles form a ring-like pattern during drying. By selecting the optimal region within this ring, consistent and reproducible measurements can be achieved.[23]

2.6. Spectrum pretreatment

The collected spectra were processed using a polynomial fitting algorithm for baseline correction and a Savitzky-Golay filter for smoothing.[24] This approach ensured spectral consistency while maintaining the linear relationship between signal intensity, laser power, and integration time, and effectively reduced noise. Subsequently, to ensure comparability among different variables, the spectra were normalized, allowing features within the same range to be standardized.

2.7. Deep learning model architecture and model training

The RamanNet architecture was utilized for classification tasks.[25] A multi-layer perceptron (MLP) was constructed for this purpose, consisting of two dense layers with batch normalization and an output layer. The Raman spectra were segmented into multiple overlapping fragments, with each fragment normalized and feature-extracted through an independent dense layer. The features obtained from all dense layers were concatenated and regularized using a dropout layer.

To optimize the multi-class microbial identification models, hyperparameters were adjusted through grid search applied to the training dataset. The training data were divided randomly into an 80:20 split for training and validation. Model selection was based on the weighted F1-score calculated from the validation set. All training and evaluations were performed using TensorFlow (version 2.9.1), Keras (version 2.9.0), and scikit-learn (version 1.3.2) on a system equipped with an Intel Core i7-14700K CPU, 128 GB RAM, and an NVIDIA GeForce RTX 4090 GPU.[26,27]

2.8. SHAP value analysis for feature importance

To identify key Raman spectral features distinguishing different bacterial species, SHapley Additive exPlanations (SHAP) analysis (version: 0.44.1) was performed.[28] SHAP values quantify the contribution of each feature to the model's predictions. By calculating the mean absolute SHAP values, the most significant Raman spectral features influencing the bacterial identification model's decisions were determined. These SHAP values were then mapped to their corresponding Raman shift positions for visualization. The SHAP values were then compared with Raman shift intensity of the testing samples for each species, revealing that the presence of several significant Raman shift peaks influenced the model's predictions.

2.9. Clinical identification data analysis

During model evaluation, the optimized model predicted the scores for 20 Raman spectra per sample. The average of these scores was calculated as the species identification score for the sample, with a classification threshold set at 0.6. The performance of the model was evaluated using several metrics, including accuracy, recall (sensitivity), precision, and F1 score. These metrics were calculated based on the confusion matrix.

3. Results

3.1. Collection of clinical isolates for AIRDIS evaluation

The isolates were identified and validated using the clinical standard method, MALDI-TOF MS. After acquiring the Raman spectra, data preprocessing was performed using the AIRDIS software to ensure data consistency. Each bacterial sample in the dataset was measured with a minimum of 20 spectra (Table 1).

3.2. Performance of Gram-positive and Gram-negative bacteria identification

This study developed a multiclass deep learning model leveraging Raman spectroscopy to identify five bacterial species: *S. aureus* and *E. faecium* (Gram-positive), as well as *K. pneumoniae*, *P. aeruginosa*, and *A. baumannii* (Gram-negative). We first developed a model to distinguish between Gram-positive and Gram-negative bacteria. As shown in Fig. 3A, the model demonstrated exceptional performance in distinguishing Gram-positive and Gram-negative bacteria, achieving an area under the curve (AUC) of 0.99, indicative of highly accurate classification. Confusion matrix analysis further confirmed strong results, with Gram-positive bacteria showing an accuracy, recall, precision, and F1 score of 97.64 %, 97.64 %, 98.36 %, and 98.00 %, respectively (Fig. 3B and Table 2). For Gram-negative bacteria, the corresponding metrics were 98.86 %, 98.86 %, 98.36 %, and 98.61 %. These findings highlight the model's reliability and robust predictive capability.

We further analyzed the spectral differences between Gram-positive and Gram-negative bacteria, as shown in Fig. 4A. Several regions with significant variation were identified, particularly the gray-shaded areas in Fig. 4A, which serve as distinguishing spectral features for

Table 2
Model performances of identifications for clinical isolates.

Bacteria classification/species (no. of isolates)	Data segment	Metrics (%)			
		Accuracy	Recall	Precision	F1
Gram positive bacteria (1,779)	Testing 1779 isolates/ 35580 RS files	97.64	97.64	98.36	98.00
S. aureus (1,015)	Testing 1015 isolates/ 20300 RS files	96.85	96.85	98.10	97.47
E. faecium (764)	Testing 764 isolates/ 15280 RS files	96.60	96.60	96.60	96.60
Gram negative bacteria (2,554)	Testing 2554 isolates/ 51080 RS files	98.86	98.86	98.36	98.61
K. pneumoniae (1,092)	Testing 1092 isolates/ 21840 RS files	96.61	96.61	95.05	95.82
P. aeruginosa (820)	Testing 820 isolates/ 16400 RS files	94.76	94.76	98.11	96.40
A. baumannii (642)	Testing 642 isolates/ 12840 RS files	96.88	96.88	93.53	95.18

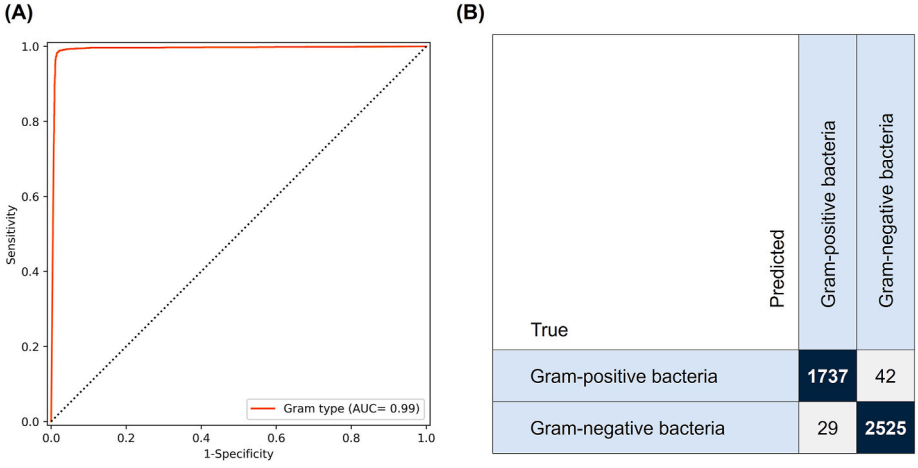

Fig. 3. Binary classification results of Gram-positive and Gram-negative bacteria. (A) The ROC curve with an AUC of 0.99. (B) The confusion matrix displaying the prediction accuracies for Gram-positive and Gram-negative bacteria, at 97.64 % and 98.86 %, respectively.

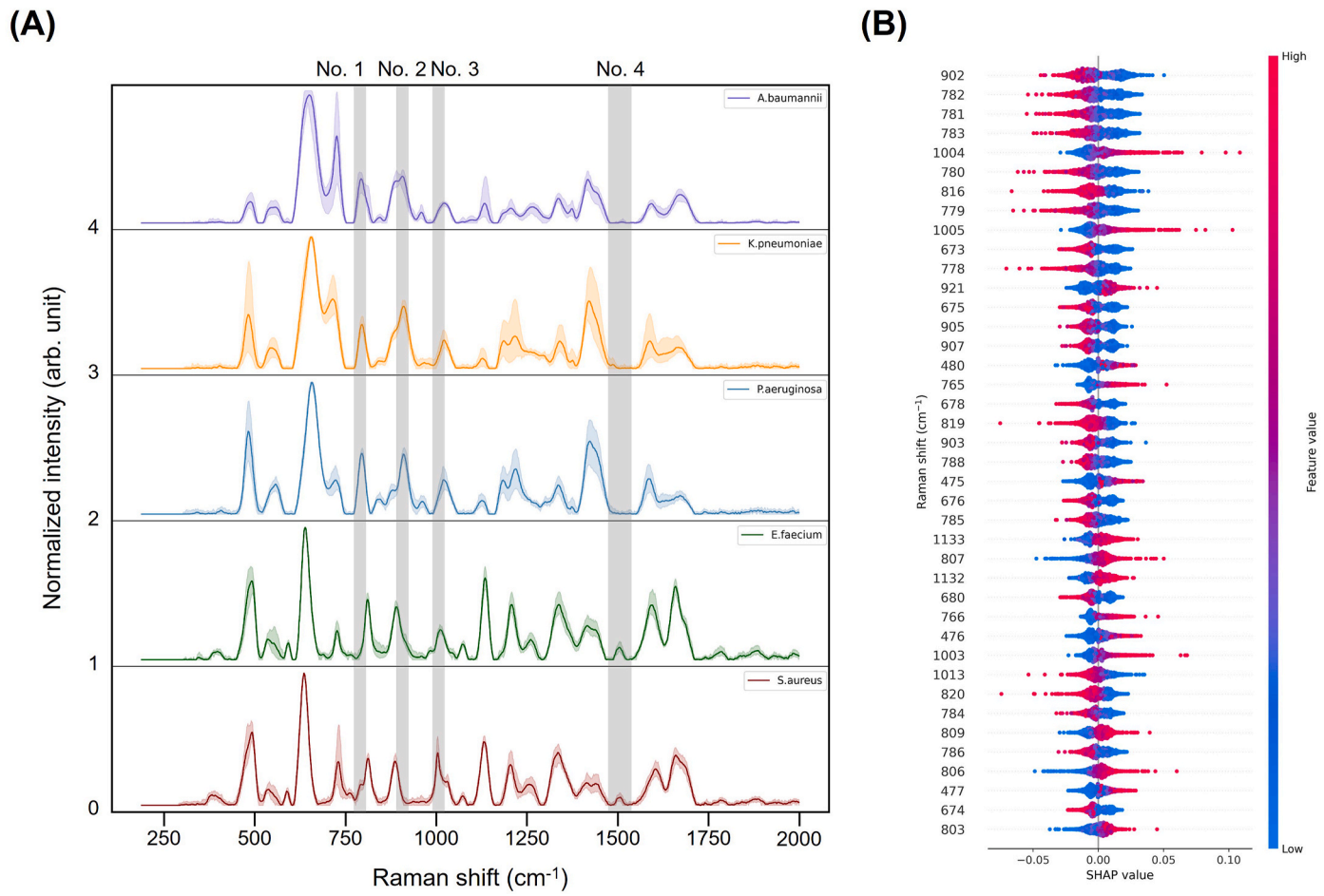

Fig. 4. Key spectral differences and features in Gram classification. (A) The spectral differences between Gram-positive and Gram-negative bacteria. (B) The 40 features which contribute the most to the outcome of the Gram classification model. Raman shift features are ranked based on their mean absolute SHAP values. Positive SHAP values contribute to the classification of spectra as belonging to Gram-positive, while negative SHAP values are associated with Gram-negative. The color bar represents the relatively higher or lower spectral intensity of the Raman shift features.

differentiating Gram-positive and Gram-negative bacteria.

Bacterial Raman spectral features primarily reflect the structural characteristics of their cell surfaces.[29,30] The principle behind Gram classification is based on the differences in the bacterial cell wall structure, which accounts for the high accuracy of the classification model in distinguishing Gram-positive and Gram-negative bacteria. For instance, the peak observed at 908 cm^{-1} in Gram-negative bacteria (region No. 2 in Fig. 4A) has been linked to saccharides, a feature attributed to molecules such as lipopolysaccharides (LPS) found on the outer membrane of Gram-negative bacteria, which are less pronounced in Gram-positive bacteria.[31,32] In contrast, the peak at 1507 cm^{-1} in Gram-positive bacteria (region No. 4 in Fig. 4A) is associated with the peptidoglycan layer of the cell wall, which is more extensive in Gram-positive bacteria. This results in a stronger Raman signal, whereas Gram-negative bacteria, with their additional outer membrane, exhibit weaker excitation of this signal, leading to differences in the spectral data.[31,33] In addition, the SHAP analysis results revealed that Raman shift features within the spectral regions of 902–907 cm^{-1}, 779–783 cm^{-1}, and 1004–1005 cm^{-1} were identified as the most significant contributors to the predictions of the Gram classification model (Fig. 4B). These finding correspond to the spectral differences observed in Fig. 4A, specifically in regions No. 1, No. 2, and No. 3, where notable variations in spectral intensity and peak positions can be observed. Spectra exhibiting peaks within the ranges of 779–783 cm^{-1} (region No. 1) and 902–907 cm^{-1} (region No. 2) are characteristic of Gram-negative bacteria, whereas spectra with peak observed in the range of 1004–1005 cm^{-1} (region No. 3) are associated with Gram positive bacteria. These differences highlight the relationship between the identified Raman shift features and the underlying structural and compositional distinctions between Gram-positive and Gram-negative bacteria, further validating the classification model's predictions.

3.3. Performance of *S. aureus* and *E. faecium* identification

In the species-level classification model, the identification of *S. aureus* and *E. faecium* demonstrated exceptional performance, with both achieving an AUC of 0.99, indicating highly accurate results (Fig. 5A). The confusion matrix confirmed these strong results. For *S. aureus*, the accuracy, recall, precision, and F1 score were 96.85 %, 96.85 %, 98.10 %, and 97.74 %, respectively (Fig. 5B and C and Table 2). Similarly, *E. faecium* achieved an accuracy, recall, precision, and F1 score of 96.60 %, 96.60 %, 96.60 %, and 96.60 %, respectively (Fig. 5B and Table 2).

We also leveraged SHAP values to investigate potentially significant spectral features or regions. An analysis was conducted on *S. aureus* and *E. faecium*, both classified as Gram-positive bacteria, identifying the top 40 most significant Raman shift features ranked by mean absolute SHAP values (Fig. 6A). This reveals that Raman shift features at 717–734 cm^{-1}, 1131–1140 cm^{-1}, and 1077–1079 cm^{-1} are the most critical for predictions in both species. A detailed examination of Fig. 6B and C reveals that spectra exhibiting higher intensity within the range of 728–734 cm^{-1} are more likely to be associated as *S. aureus*. In contrast, spectra

(A)

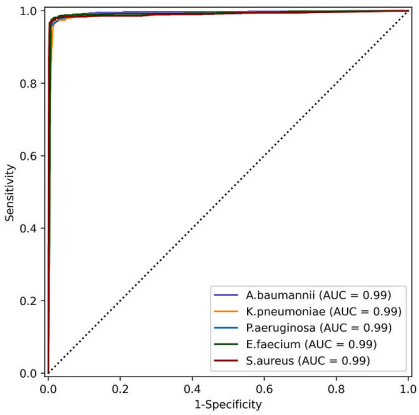

(B)

True \ Predicted	*S. aureus*	*E. faecium*	*K. pneumoniae*	*P. aeruginosa*	*A. baumannii*
S. aureus	**983**	7	14	0	11
E. faecium	9	**738**	11	3	3
K. pneumoniae	4	10	**1055**	10	13
P. aeruginosa	5	8	14	**777**	16
A. baumannii	1	1	16	2	**622**

(C)

True \ Predicted	*S. aureus*	*E. faecium*	*K. pneumoniae*	*P. aeruginosa*	*A. baumannii*
S. aureus	**96.85**	0.69	1.38	0.00	1.08
E. faecium	1.18	**96.60**	1.44	0.39	0.39
K. pneumoniae	0.37	0.92	**96.61**	0.92	1.19
P. aeruginosa	0.61	0.98	1.71	**94.76**	1.95
A. baumannii	0.16	0.16	2.49	0.31	**96.88**

Fig. 5. Binary classification results of species identification. (A) AUC for the deep learning algorithm in species identification. The confusion matrix displaying (B) prediction results and (C) prediction accuracies (%) for *S. aureus*, *E. faecium, K. pneumoniae*, *P. aeruginosa*, and *A. baumannii* (96.85, 96.60, 96.61, 94.76, and 96.88, respectively).

with higher intensity within the ranges of 717–726 cm^{-1}, 1131–1140 cm^{-1} and 1077–1079 cm^{-1} are indicative of *E. faecium*.

These findings closely correspond to the observed spectral characteristics. As illustrated in Fig. 7A, the gray-shaded regions highlight the spectral differences between the two species. While the variation in region No. 2 appears subtle, a comparison with the peak at 490–500 cm^{-1} suggests that the relative intensity differences between adjacent peaks could be crucial in improving classification accuracy.

3.4. Performance of *K. pneumoniae, P. aeruginosa and A. baumannii* identification

For Gram-negative bacteria, including *K. pneumoniae*, *P. aeruginosa*, and *A. baumannii*, the model achieved an AUC of 0.99 for each, demonstrating its exceptional performance (Fig. 5A). The classification metrics demonstrated similarly strong performance in Gram-negative bacteria (Fig. 5B and Table 2). *K. pneumoniae* achieved 96.61 % accuracy, 96.60 % recall, 95.05 % precision, and a 95.82 % F1 score. For *P. aeruginosa*, the values were 94.76 %, 94.76 %, 98.11 %, and 96.40 %, respectively. *A. baumannii* attained 96.88 % accuracy, 96.88 % recall, 93.53 % precision, and a 95.18 % F1 score. These findings provide strong evidence supporting the model's reliability and its robust predictive capability in accurately distinguishing between Gram-positive and Gram-negative bacteria.

Similarly, we conducted SHAP value analysis on Gram-negative bacteria, including *K. pneumoniae*, *P. aeruginosa*, and *A. baumannii*, to identify potentially significant spectral features or regions. Fig. 6D show the top 40 most important Raman shift features ranked by mean absolute SHAP values. The results indicate that Raman shift features at 1128–1138 cm^{-1}, 678–682 cm^{-1}, and 713–738 cm^{-1} contributed the most to predictions for these three bacterial species. A closer examination of Fig. 6E to G reveals that spectra with higher intensity in the ranges of 1128–1138 cm^{-1} and 713–738 cm^{-1} are more likely to be associated as *K. pneumoniae*. In contrast, spectra with higher intensity within the ranges of 853–861 cm^{-1} and 1173–1176 cm^{-1} are indicative of *P. aeruginosa*. Additionally, spectra exhibiting higher intensity within the ranges of 673–682 cm^{-1}, 722–725 cm^{-1} and 1373–1374 cm^{-1} are characteristic of *A. baumannii*.

In the Raman spectra, although Gram-negative bacteria share common characteristic features, the gray-shaded regions in Fig. 7B highlight significant spectral differences among the three species. These differences are reflected in the varying expression levels of specific features, which, in turn, influence the relative intensity between adjacent peaks. Such variations may play a critical role in improving classification accuracy. Additionally, we observed that the predictive impact of individual features varied across different bacterial species. For instance, the Raman shift feature at 678 cm^{-1} had a stronger influence on the predictions for *A. baumannii* and *K. pneumoniae*, while its impact on *P. aeruginosa* was comparatively smaller. This variation is visually evident in the different sizes of the color-coded regions corresponding to each species. Conversely, the Raman shift feature at 861 cm^{-1} demonstrated greater importance for *P. aeruginosa* and *K. pneumoniae*, while its contribution to *A. baumannii* predictions was less significant.

These findings provide strong evidence supporting the model's reliability and its robust predictive capability in accurately distinguishing between Gram-positive and Gram-negative bacteria.

4. Discussion

This study developed an identification system integrating Raman spectroscopy and ML for *S. aureus*, *E. faecium*, *K. pneumoniae*, *P. aeruginosa*, and *A. baumannii*. According to the World Health Organization's 2024 bacterial priority pathogens list, these bacteria are classified under the priority categories of either the critical or high group.[34] Specifically, carbapenem-resistant *K. pneumoniae*, *A. baumannii*, and *P. aeruginosa* (CRKP, CRAB, and CRPA) rank 1st, 3rd, and 10th, respectively. Vancomycin-resistant *E. faecium* (VRE) and methicillin-resistant *S. aureus* (MRSA) rank 9th and 14th overall, and 1st and 3rd among Gram-positive bacteria. This underscores the critical importance of rapid and accurate identification of these bacterial species, as well as understanding their antimicrobial resistance. The AIRDIS developed in this study demonstrated excellent performance in identifying these five bacterial species, providing significant support for the future development of antimicrobial resistance prediction models.

The potential clinical applications of Raman spectroscopy have been extensively investigated in research. SERS effectively addresses challenges such as weak signals and low reproducibility, significantly enhancing its utility in clinical settings.[35] However, due to the complexity of the data, ML is now considered essential for the analysis of Raman spectral signals.[36] Numerous studies have explored the effectiveness of combining SERS technology with ML algorithms for the rapid detection of bacteria.[16,17,37,38] In 2021, Tang et al. analyzed 117 isolates from nine clinically significant *Staphylococcus* species, achieving an accuracy of 98.21 %.[37] In 2022, Tang et al. utilized SERS combined with machine learning to distinguish 103 clinical bacterial isolates from 15 species, including *Achromobacter xylosoxidans*, achieving an accuracy of 99.86 %.[38] In 2022, Wang et al. analyzed 30 bacterial species from 9 different genera, achieving an accuracy of 99.80 % at the genus level and 98.37 % at the species level.[16] A more recent study analyzing 30 bacterial species reported an overall accuracy of 90.55 %.[17] However, a

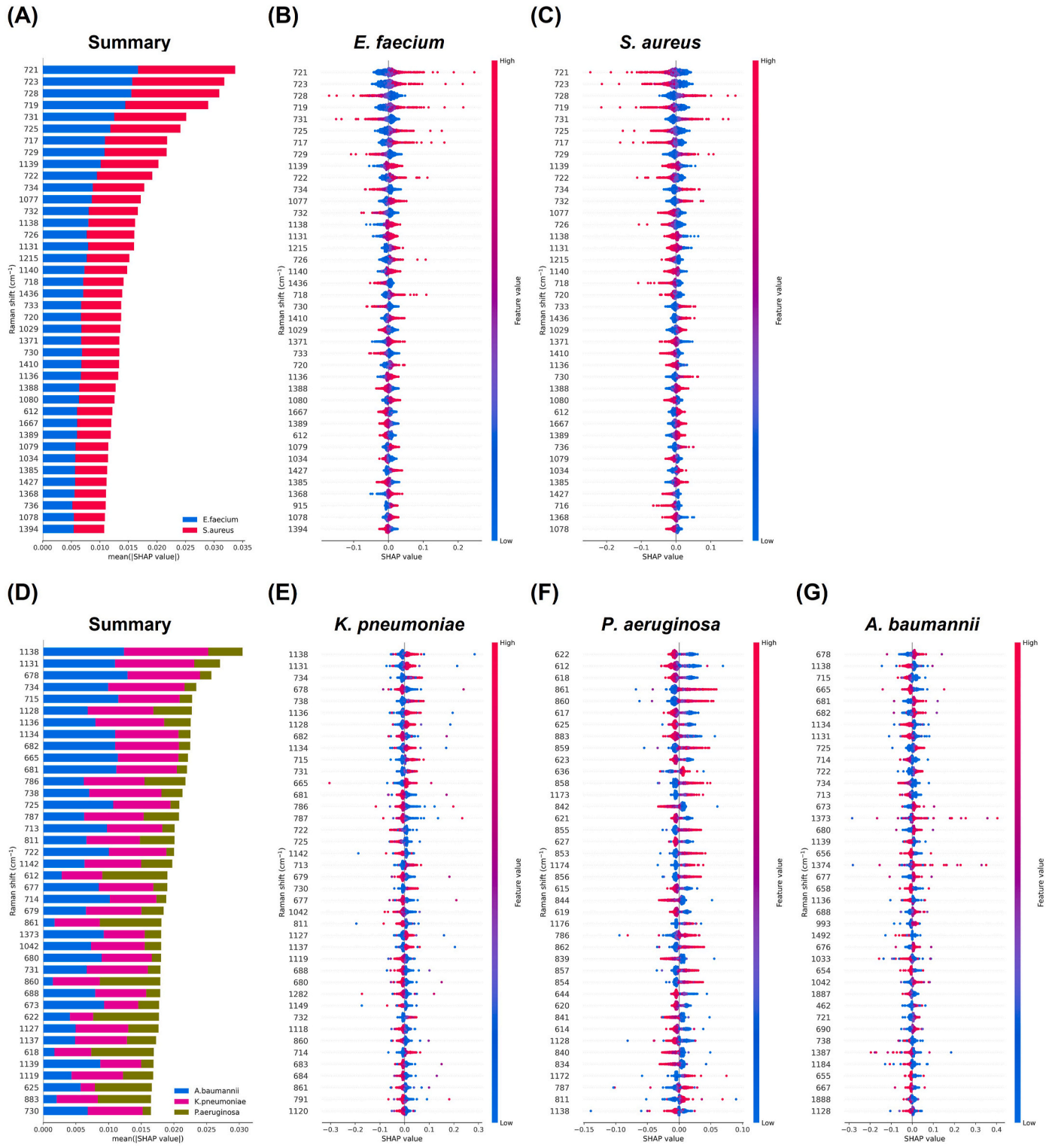

Fig. 6. The 40 features contributing the most to the outcomes of classification models for (A) Gram-positive bacteria (B) *S. aureus*, (C) *E. faecium*, (D) Gram-negative bacteria, (E) *K. pneumoniae*, (F) *P. aeruginosa*, and (G) *A. baumannii*. Raman shift features are ranked based on their mean absolute SHAP values. In panels (B), (C), (E), (F) and (G), positive SHAP values contribute to the classification of spectra as belonging to their respective classes, while negative SHAP values indicate the opposite. The color bar represents the relatively higher or lower spectral intensity of the Raman shift features.

significant gap is still widely recognized between basic research and practical applications.[35] While the studies mentioned above achieved promising results, they were limited by the relatively small number of isolates analyzed, despite generating over ten thousand spectra. The variability among clinical isolates remains a major challenge for broader application. The AIRDIS developed in this study utilized 5554 clinical isolates during training and testing, generating a total of 197,740 Raman spectra. It achieved an accuracy of over 94.76 % across various classification tasks. Furthermore, the system was seamlessly integrated into the workflow of a clinical microbiology laboratory, demonstrating the

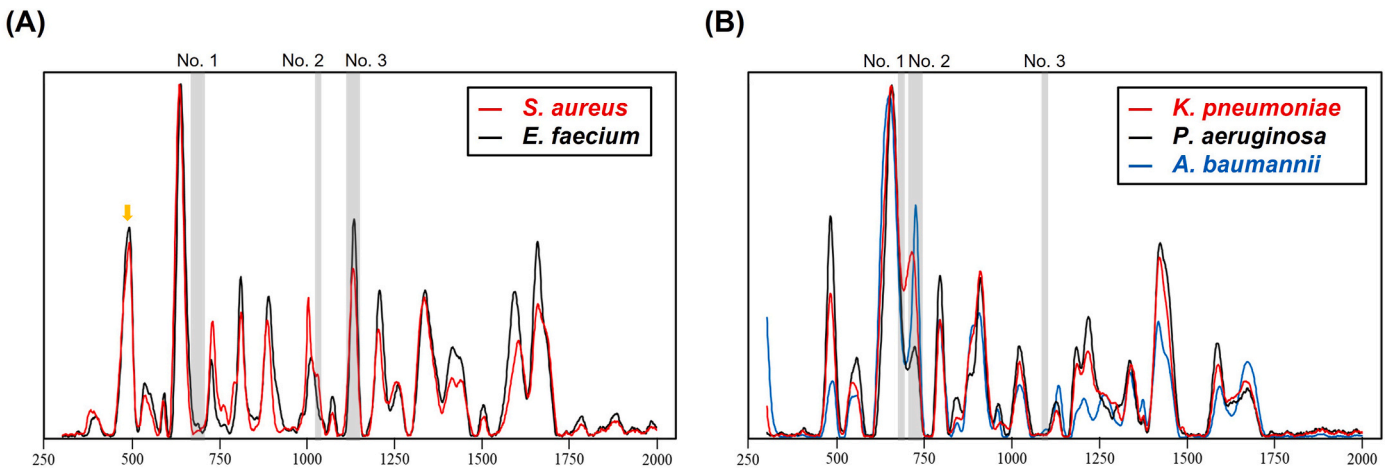

Fig. 7. The spectral differences among 5 species. (A) *S. aureus* and *E. faecium* (B) *K. pneumoniae*, *P. aeruginosa*, and *A. baumannii*. Gray-shaded areas indicate significant variations. The arrow indicates the peak at 490–500 cm^{-1}.

practical applicability of combining SERS with machine learning in clinical settings.

Previous studies have reported significant differences in peaks at 540 and 1380 cm^{-1} when comparing Gram-positive and Gram-negative bacteria. This feature is primarily attributed to glycosidic bonds in *N*-acetyl glucosamine and *N*-acetyl muramic acid of peptidoglycan.[31] However, in the SHAP analysis conducted in this study, these two peaks were not identified as key features. Instead, we observed that the most pronounced difference between Gram-positive and Gram-negative bacteria was the peak at 908 cm^{-1}, which is associated with LPS present in the outer membrane of Gram-negative bacteria.[31,32] As LPS are an outer membrane structure exclusively found in Gram-negative bacteria, their use as a primary feature to distinguish between Gram-positive and Gram-negative bacteria is theoretically justified. It is important to note that bacteria possess various mechanisms for LPS modification.[39] For instance, *P. aeruginosa* may modify its lipid A during long-term chronic infection to enhance immune evasion. Similarly, *Burkholderia dolosa* has been observed to alter its O-antigen structure during infection, potentially promoting biofilm formation. Additionally, *Burkholderia cenocepacia* has been found to exhibit O-antigen deficiency, which increases macrophage internalization following phagocytosis. *Helicobacter pylori* can also modify its LPS to evade immune responses, thereby sustaining infection. More importantly, LPS modification is one of the resistance mechanisms employed by bacteria such as *K. pneumoniae*, *P. aeruginosa*, *A. baumannii*, and *Salmonella* against polymyxin B or colistin.[40] This highlights the importance of evaluating the performance of the AIRDIS when encountering such isolates. Moreover, attention should be given to whether these factors could impact identification performance in future developments of antimicrobial resistance prediction systems.

Due to the variability of clinical bacteria, different strains of the same species may exhibit distinct features in their Raman spectra. To minimize the issue of strain specificity, we utilized isolates from the SMART program, which includes isolates collected from 18 major hospitals across Taiwan. However, it is important to note that all isolates in this study originated from Taiwan, which represents a limitation of this research.

Compared to the commonly used MALDI-TOF MS in clinical microbiology laboratories, the AIRDIS requires a similar operation time (average 1–3 min per sample). However, the cost per sample, instrument price, and maintenance expenses for AIRDIS are significantly lower than those of MALDI-TOF MS. In terms of accuracy, MALDI-TOF MS achieves nearly 100 % accuracy for *S. aureus*, *E. faecium*, *K. pneumoniae*, and *P. aeruginosa*, but its accuracy for *A. baumannii* is relatively lower at approximately 89.7 %. In contrast, AIRDIS demonstrated accuracies ranging from 94.76 % to 98.86 % across all five species. These results highlight AIRDIS as a competitive option, particularly for small-to medium-sized hospitals.

In conclusion, the AIRDIS offers rapid, accurate, and cost-effective bacterial identification while seamlessly integrating into the workflow of clinical microbiology laboratories. Validated with a large number of isolates, it demonstrated excellent performance in identifying clinically significant species, including *S. aureus*, *E. faecium*, *K. pneumoniae*, *P. aeruginosa*, and *A. baumannii*. This study provides valuable insights for advancing Raman technology as an alternative method for bacterial identification and for developing antimicrobial resistance prediction systems in the future.

CRediT authorship contribution statement

Yu-Tzu Lin: Writing – original draft, Visualization, Validation, Supervision, Software, Resources, Project administration, Methodology, Investigation, Funding acquisition, Formal analysis, Data curation, Conceptualization. **Hsiu-Hsien Lin:** Software, Resources, Project administration, Methodology, Investigation, Formal analysis, Data curation, Conceptualization. **Chih-Hao Chen:** Supervision, Software, Resources, Project administration, Methodology, Investigation, Funding acquisition, Formal analysis. **Kun-Hao Tseng:** Visualization, Validation, Supervision, Software, Resources, Project administration, Methodology, Investigation, Funding acquisition, Formal analysis, Data curation. **Pang-Chien Hsu:** Visualization, Validation, Supervision, Software, Resources, Project administration, Methodology, Investigation, Funding acquisition, Formal analysis, Data curation. **Ya-Lun Wu:** Visualization, Validation, Supervision, Resources, Project administration, Methodology, Investigation, Funding acquisition, Data curation. **Wei-Cheng Chang:** Software, Investigation, Data curation, Conceptualization. **Nai-Shun Liao:** Resources, Methodology, Investigation, Data curation. **Yi-Fan Chou:** Methodology, Investigation, Data curation. **Chun-Yi Hsu:** Methodology, Investigation, Data curation. **Yu-Hui Liao:** Methodology, Investigation, Data curation. **Mao-Wang Ho:** Supervision, Software, Resources, Project administration, Methodology, Investigation, Formal analysis, Data curation. **Shih-Sheng Chang:** Visualization, Validation, Supervision, Software, Resources, Project administration, Methodology, Investigation, Formal analysis, Data curation. **Po-Ren Hsueh:** Writing – review & editing, Writing – original draft, Visualization, Validation, Supervision, Software, Resources, Project administration, Methodology, Investigation, Funding acquisition, Formal analysis, Data curation, Conceptualization. **Der-Yang Cho:** Visualization, Validation, Supervision, Software, Resources, Project administration, Methodology, Investigation, Funding acquisition, Formal analysis, Data curation, Conceptualization.

Funding

This study was supported by the grant NSTC 112-2320-B-039-053 from the National Science and Technology Council of Taiwan and CMU112-MF-63 from China Medical University, Taichung, Taiwan.

Declaration of competing interest

The authors declare no conflict of interest.

Acknowledgments

Investigators from the SMART program 2017–2020: Wen-Sen Lee (Wan Fang Hospital, Taipei), Min-Chi Lu (China Medical University Hospital, Taichung), Zhi-Yuan Shi (Taichung Veterans General Hospital, Taichung), Yao-Shen Chen (Kaohsiung Veterans General Hospital, Kaohsiung), Lih-Shinn Wang (Buddhist Tzu Chi General Hospital, Hualien), Shu-Hui Tseng (Ministry of Health and Welfare, Taipei), Chao-Nan Lin (National Pingtung University of Science and Technology, Pingtung), Yin-Ching Chuang (Chi Mei Hospital, Tainan), Yu-Hui Chen (Chi Mei Hospital, Tainan), Wang-Huei Sheng (National Taiwan University Hospital, Taipei), Chang-Pan Liu (MacKay Memorial Hospital, Taipei), Ting-Shu Wu (Chang Gung Memorial Hospital, Taoyuan), Chun-Ming Lee (St Joseph's Hospital, Yunlin), Po-Liang Lu (Kaohsiung Medical University Hospital, Kaohsiung), Muh-Yong Yen (Taipei City Hospital, Taipei), Pei-Lan Shao (National Taiwan University Hospital, Hsin-Chu), Shu-Hsing Cheng (Taoyuan General Hospital, Taoyuan), Chi-Ying Lin (National Taiwan University Hospital, Yun-Lin), Ming-Huei Liao (National Pingtung University of Science and Technology, Pingtung), Yen-Hsu Chen (Kaohsiung Medical University, Kaohsiung), Wen-Chien Ko (National Cheng Kung University Hospital, Tainan), Fu-Der Wang (Taipei Veterans General Hospital, Taipei) and Po-Ren Hsueh (China Medical University Hospital, Taichung. Taiwan).

References

1. Collaborators GBDAR. Global mortality associated with 33 bacterial pathogens in 2019: a systematic analysis for the Global Burden of Disease Study 2019. *Lancet*. 2022;400:2221–2248.
2. World Health O. *Global Report on the Epidemiology and Burden of Sepsis: Current Evidence, Identifying Gaps and Future Directions*. Geneva: World Health Organization; 2020.
3. Diseases GBD, Injuries C. Global burden of 369 diseases and injuries in 204 countries and territories, 1990-2019: a systematic analysis for the Global Burden of Disease Study 2019. *Lancet*. 2020;396:1204–1222.
4. Davenport M, Mach KE, Shortliffe LMD, Banaei N, Wang TH, Liao JC. New and developing diagnostic technologies for urinary tract infections. *Nat Rev Urol*. 2017;14:296–310.
5. Maugeri G, Lychko I, Sobral R, Roque ACA. Identification and antibiotic-susceptibility profiling of infectious bacterial agents: a review of current and future trends. *Biotechnol J*. 2019;14, e1700750.
6. Yu J, Lin HH, Tseng KH, et al. Prediction of methicillin-resistant *Staphylococcus aureus* and carbapenem-resistant *Klebsiella pneumoniae* from flagged blood cultures by combining rapid Sepsityper MALDI-TOF mass spectrometry with machine learning. *Int J Antimicrob Agents*. 2023;62, 106994.
7. Lee KS, Landry Z, Pereira FC, et al. Raman microspectroscopy for microbiology. *Nat Rev Methods Primers*. 2021;1:80.
8. Dina NE, Zhou H, Colnita A, et al. Rapid single-cell detection and identification of pathogens by using surface-enhanced Raman spectroscopy. *Analyst*. 2017;142:1782–1789.
9. Ho CS, Jean N, Hogan CA, et al. Rapid identification of pathogenic bacteria using Raman spectroscopy and deep learning. *Nat Commun*. 2019;10:4927.
10. Magdy M. A conceptual overview of surface-enhanced Raman scattering (SERS). *Plasmonics*. 2023;18:803–809.
11. Geraldes C. Introduction to infrared and Raman-based biomedical molecular imaging and comparison with other modalities. *Molecules*. 2020;25.
12. Akanny E, Bonhommé A, Bessueille F, Bourgeois S, Bordes C. Surface enhanced Raman spectroscopy for bacteria analysis: a review. *Appl Spectrosc Rev*. 2021;56:380–422.
13. Petry R, Schmitt M, Popp J. Raman spectroscopy–a prospective tool in the life sciences. *ChemPhysChem*. 2003;4:14–30.
14. Fleischmann M, Hendra PJ, McQuillan AJ. Raman spectra of pyridine adsorbed at a silver electrode. *Chem Phys Lett*. 1974;26:163–166.
15. Zhou B, Tong YK, Zhang R, Ye A. RamanNet: a lightweight convolutional neural network for bacterial identification based on Raman spectra. *RSC Adv*. 2022;12:26463–26469.
16. Wang L, Tang JW, Li F, et al. Identification of bacterial pathogens at genus and species levels through combination of Raman spectrometry and deep-learning algorithms. *Microbiol Spectr*. 2022;10, e0258022.
17. Liu Y, Gao Y, Niu R, et al. Rapid and accurate bacteria identification through deep-learning-based two-dimensional Raman spectroscopy. *Anal Chim Acta*. 2024;1332, 343376.
18. Jean SS, Ko WC, Hsueh PR, Group SS. Susceptibility of clinical isolates of meticillin-resistant *Staphylococcus aureus* and phenotypic non-extended-spectrum β-lactamase-producing *Klebsiella pneumoniae* to ceftaroline in Taiwan: results from antimicrobial testing leadership and surveillance (ATLAS) in 2012-2018 and Surveillance of multicentre Antimicrobial Resistance in Taiwan (SMART) in 2018-2019. *Int J Antimicrob Agents*. 2020;56, 106016.
19. Liu PY, Lee YL, Lu MC, et al. National surveillance of antimicrobial susceptibility of bacteremic gram-negative bacteria with emphasis on community-acquired resistant isolates: report from the 2019 Surveillance of Multicenter Antimicrobial Resistance in Taiwan (SMART). *Antimicrob Agents Chemother*. 2020;64.
20. Chen CH, Wu PH, Lu MC, Ho MW, Hsueh PR, Group SPS. National surveillance of antimicrobial susceptibilities to ceftaroline, dalbavancin, telavancin, tedizolid, eravacycline, omadacycline, and other comparator antibiotics, and genetic characteristics of bacteremic *Staphylococcus aureus* isolates in adults: results from the Surveillance of Multicenter Antimicrobial Resistance in Taiwan (SMART) program in 2020. *Int J Antimicrob Agents*. 2023;61, 106745.
21. Lee Y-L, Liu C-E, Tang H-J, et al. Epidemiology and antimicrobial susceptibility profiles of enterobacterales causing bloodstream infections before and during COVID-19 pandemic: results of the study for monitoring antimicrobial resistance trends (SMART) in Taiwan, 2018–2021. *J Microbiol Immunol Infect*. 2024;57:446–456.
22. Hunter R, Sohi AN, Khatoon Z, et al. Optofluidic label-free SERS platform for rapid bacteria detection in serum. *Sensor Actuator B Chem*. 2019;300, 126907.
23. Zhu Q, Li X, Li D, Lu F, Zhao Y, Yuan Y. A rapid therapeutic drug monitoring strategy of carbamazepine in serum by using coffee-ring effect assisted surface-enhanced Raman spectroscopy. *Molecules*. 2022;28.
24. Zimmermann B, Kohler A. Optimizing Savitzky-Golay parameters for improving spectral resolution and quantification in infrared spectroscopy. *Appl Spectrosc*. 2013;67:892–902.
25. Ibtehaz N, Chowdhury MEH, Khandakar A, Kiranyaz S, Rahman MS, Zughaier SM. RamanNet: a generalized neural network architecture for Raman spectrum analysis. *Neural Comput Appl*. 2023;35:18719–18735.
26. Zollanvari A. Deep learning with keras-TensorFlow. In: Zollanvari A, ed. *Machine Learning with Python: Theory and Implementation*. Cham: Springer International Publishing; 2023:351–391.
27. Raschka S, Liu YH, Mirjalili V. *Machine Learning with PyTorch and Scikit-Learn: Develop Machine Learning and Deep Learning Models with Python*. Packt Publishing Ltd; 2022.
28. Lundberg SM, Lee S-I. A unified approach to interpreting model predictions. *Adv Neural Inf Process Syst*. 2017;30:4765–4774.
29. Mosier-Boss PA. Review on SERS of bacteria. *Biosensors*. 2017;7.
30. Hassan M, Zhao Y, Zughaier SM. Recent advances in bacterial detection using surface-enhanced Raman scattering. *Biosensors*. 2024;14.
31. de Siqueira EOFS, da Silva AM, Pacheco MTT, Giana HE, Silveira Jr L. Biochemical characterization of pathogenic bacterial species using Raman spectroscopy and discrimination model based on selected spectral features. *Laser Med Sci*. 2021;36:289–302.
32. Uchiyama T, Sonoyama M, Hamada Y, et al. Raman spectroscopic study on the L-type straight flagellar filament of *Salmonella*. *Vib Spectrosc*. 2006;42:192–194.
33. Sengupta A, Brar N, Davis EJ. Bioaerosol detection and characterization by surface-enhanced Raman spectroscopy. *J Colloid Interface Sci*. 2007;309:36–43.
34. Jesudason T. WHO publishes updated list of bacterial priority pathogens. *Lancet Microbe*. 2024;5, 100940.
35. Wang L, Liu W, Tang JW, et al. Applications of Raman spectroscopy in bacterial infections: principles, advantages, and shortcomings. *Front Microbiol*. 2021;12, 683580.
36. Bocklitz T, Walter A, Hartmann K, Rösch P, Popp J. How to pre-process Raman spectra for reliable and stable models? *Anal Chim Acta*. 2011;704:47–56.
37. Tang JW, Liu QH, Yin XC, et al. Comparative analysis of machine learning algorithms on surface enhanced Raman spectra of clinical *Staphylococcus* species. *Front Microbiol*. 2021;12, 696921.
38. Tang JW, Li JQ, Yin XC, et al. Rapid discrimination of clinically important pathogens through machine learning analysis of surface enhanced Raman spectra. *Front Microbiol*. 2022;13, 843417.
39. Maldonado RF, Sa-Correia I, Valvano MA. Lipopolysaccharide modification in Gram-negative bacteria during chronic infection. *FEMS Microbiol Rev*. 2016;40:480–493.
40. Hamel M, Rolain JM, Baron SA. The history of colistin resistance mechanisms in bacteria: progress and challenges. *Microorganisms*. 2021;9:442.